MASTERARBEIT | MASTER'S THESIS

Titel | Title

Investigation of the pro-inflammatory effects of micro- & nanoplastic particles on different cancer cell lines in vitro

verfasst von | submitted by

Matea Stojanovic BSc

angestrebter akademischer Grad | in partial fulfilment of the requirements for the degree of

Magistra pharmaciae (Mag. pharm.)

Wien | Vienna, 2024

Studienkennzahl lt. Studienblatt | Degree programme code as it appears on the student record sheet:	UA 066 605
Studienrichtung lt. Studienblatt | Degree programme as it appears on the student record sheet:	Masterstudium Pharmazie
Betreut von | Supervisor:	Assoz. Prof. Mag. Dr. Verena Pichler

Acknowledgement

First and foremost, I would like to thank my supervisor Assoc.-Prof.in Mag.a Dr.in Verena Pichler for allowing me to be part of her amazing research group and for sharing her knowledge and expertise with me. I want to thank Mag.a pharm. Lisa Aichinger, my partner in crime through this experience. Your endless helpfulness, patience and positivity made this experience unparalleled. Thank you, Lukas Kogler, MSc. for providing me with your PET-particles and your assistance in this area. And to the rest of the team, I cannot describe how thankful I am to all of you for your hospitality and for making the last months of this chapter in my life unforgettable. I will miss you dearly.

I would like to express my heartfelt gratitude towards my family, boyfriend, and friends, whose persistent belief in me never faltered, even when I doubted myself. Your continuous support led me to this point. This is as much your achievement as it is mine. Last but not least, I want to thank the woman, who led by example, proving that with high persistence and a positive mindset, you can rise above your limits. Thank you, Mama - I know you would be proud.

Abstract

Background: The extent of environmental plastic pollution has reached an alarmingly high level. Polyethylene terephthalate (PET), a major compound packaging material, significantly contributes to this waste. Due to a range of different chemical and physical processes these plastic debris fragment into micro- and nanoplastics (MNPs), which subsequently distribute across vital resources. Consequently, humans are exposed to these plastic particles daily through ingestion and inhalation. Therefore, it has become essential to investigate the effects on human tissues. Recent studies have increasingly proven, that the induction of reactive oxygen species (ROS) by MNPs leads to a cycle of toxic effects within the body. This potentially initiates the development of chronic inflammations and diseases.

Methods: This study focuses on investigating whether heterogeneous PET-samples (< 2.5 µm) initiate oxidative stress in cells. One of the PET-samples was labeled with fluorescein for their detection under the fluorescence microscope. Cell lines representing different tissues, such as lung, colon, and fascia (H460, HCT-116, HT-29, HT-1080, NIH/3T3), were selected for the experiments. All cells, except NIH/3T3, are cancer cells. The cell inhibitory effect of both PET-particles was determined by using the MTT-assay. Subsequently, the general ROS levels were measured, followed by assessing the mitochondrial production of ROS. Both assays rely on a fluorescence-based staining method. Additionally, the impact of PET exposure on cell was investigated using a three-dimensional (3D) model.

Results: The cell viability assay revealed a dose-dependent cell inhibitory effect by PET, with almost a total loss of viable cells observed in HCT-116 cells at the highest concentration. The dose-dependency was additionally noticed for general ROS generation, with all cell lines showing a significant increase with higher doses. The mitochondrial response to PET-particles demonstrated a different pattern. The mtROS level did not correlate with the exposed concentration in a proportional manner. Spheroid growth analysis revealed no significant difference in the spheroids' sizes between PET-treated and untreated cells.

Conclusion: The data demonstrated a dose-dependent increase in general, intracellular ROS levels across all cell lines. The measurement of mitochondrial ROS showed that there is a possibility that ROS may also be generated through non-mitochondrial pathways. The MTT-assay indicated a dose-dependent loss in cell viability and confirmed the cytotoxic potential of PET-particles. These findings support the hypothesis that PET particles can induce inflammatory processes in human cells. However, further studies are necessary to narrow down the crucial factors and determine the effect on long-term exposure.

Zusammenfassung

Hintergrund: Die Umweltverschmutzung durch Plastik stellt seit Jahren ein zunehmend bedrohliches globales Problem dar. Polyethylenterephthalat (PET), ein Hauptbestandteil gängiger Verpackungsmaterialien, trägt maßgeblich zu dieser Belastung bei. Durch zahlreiche chemische und physikalische Prozesse zerfällt dieser Kunststoff in Mikro- und Nanoplastikpartikel (MNPs), die sich dann unkontrolliert in lebensnotwendige Ressourcen wie Luft, Wasser und Nahrungsmitteln verbreiten. Infolgedessen ist die tägliche Aufnahme dieser Plastikpartikeln durch Nahrung und Inhalation unausweichlich. Jüngste in-vitro Studien belegen, dass durch MNPs induzierte reaktiven Sauerstoffspezies (ROS) eine Kaskade toxischer Effekte auslösen können, die zur Entwicklung chronischer Entzündungen und Krankheiten führen.

Methoden Diese Studie untersucht, ob die Exposition mit heterogenen PET-Partikeln (jeweils < 2.5 µm) oxidativen Stress in Zellen auslöst. Eine der PET-Proben wurde mit Fluorescein markiert, um die Detektion unter dem Fluoreszenzmikroskop für gewählte Experimente zu ermöglichen. Für die in-vitro Experimente wurden Zelllinien, als Repräsentation verschiedener Gewebe, darunter Lunge, Darm und Bindegewebe (H460, HCT-116, HT-29, HT-1080, NIH/3T3), ausgewählt. Alle Zellen, ausgenommen NIH/3T3, stammen aus malignen Tumorgeweben. Die hemmende Wirkung auf die Zellviabilität der PET-Partikel wurde mittels MTT-Assay bestimmt. Durch fluoreszenzbasierte Färbemethoden wurden anschließend die allgemeinen, intrazellulären ROS-Werte gemessen, gefolgt von einer Bestimmung mitochondrialer ROS-Produktion (mtROS). Zusätzlich wurde das Zellwachstum nach PET-Exposition in einem dreidimensionalen Sphäroidmodell analysiert.

Ergebnisse: Der MTT-Assay zeigte eine dosisabhängige Minimierung der Zellviabilität. Die dosisabhängige Zunahme der allgemeinen ROS-Produktion wurde ebenfalls in allen Zelllinien beobachtet. Die mitochondriale ROS-Reaktion wiesen jedoch ein anderes Muster auf und wiesen keinen proportionalen Anstieg zwischen dem mtROS-Spiegel und der Konzentration der PET-Partikel vor. Die Analyse des Sphäroidwachstums ergab keinen signifikanten Unterschied in der Größe zwischen behandelten und unbehandelten Zellen.

Schlussfolgerung: Die Daten zeigten eine dosisabhängige Erhöhung der allgemeinen ROS-Produktion in allen untersuchten Zelllinien. Die mitochondrialen Messungen deuten darauf hin, dass ROS durch andere, nicht-mitochondriale Mechanismen, erzeugt werden könnten. Die Ergebnisse stützen die Hypothese, dass PET-Partikel entzündliche Prozesse in menschlichen Zellen induzieren können. Weitere Studien sind erforderlich, um die zugrunde liegenden Mechanismen und die Langzeitauswirkungen zu klären.

Table of content

1 Introduction

1.1 Micro- and nanoplastics

The environmental impact of plastic has become a subject of growing interest in recent years. While plastic was initially hailed as a revolutionary material in numerous industries, it has become increasingly evident that it poses a significant environmental threat due to its negligent disposal in our environment. The amount of plastic waste is rising exponentially with the society's favor for single use items, expecting an increase of about 12 billion tons of plastic waste contaminating the planet by the year 2050 [1]. The harmful effects derive from the material's chemical stability and the widespread distribution, exacerbated by uncontrollable fragmentation into micro- and nanoplastics (MNPs). Given their microscopic size, it is challenging to remove them entirely from the ecosystem with the currently given technical devices. Their presence has been found in essential resources, including groundwater, air and food [2]. Thus, there is a high risk of MNPs entering the human body.

MNPs are classified based on their origin, size, and shape. Primary microparticles are intentionally produced and are commonly found in products of every household, e.g. detergents [3] [4]. Secondary MNPs include plastic fragments from plastic products such as textiles, electronics, packaging materials, etc. [5]. While the size range of microplastics (MPs) spans from 1 to 1000 µm, the upper limit of the nanoplastics' (NP) size class is a matter of scientific debate, with proposed values ranging from 100 nm to 1000 nm [6]. Moreover, the uncontrollable degradation of plastic products results in the formation of particles with heterogeneous shape. These shapes can play a crucial role in determining the impact on human cells [1].

Once particles enter the human body via the respiratory or digestive tract, they can cause toxic effects, including inflammatory responses and oxidative stress. Studies have shown that all these responses are directly related to the pathogenesis of chronic diseases. Consequently, there is concern about the potential consequences on human health [7].

1.2 PET – from the bottle to the human cell

Polyethylene terephthalate, better known as PET, is a thermoplastic polymer, that was first synthesized in the 1940s [8]. Chemically, it is characterized by its long-chain polymers with repeating ester functional groups. The synthesis of PET is primarily achieved through a polycondensation reaction between terephthalic acid (TPA) and ethylene glycol (EG) (Figure 1). Due to its favorable physical properties, PET rapidly became the dominant material in the packaging industry, offering significant advantages in terms of weight, cost-efficiency and resilience to various weather conditions [9].

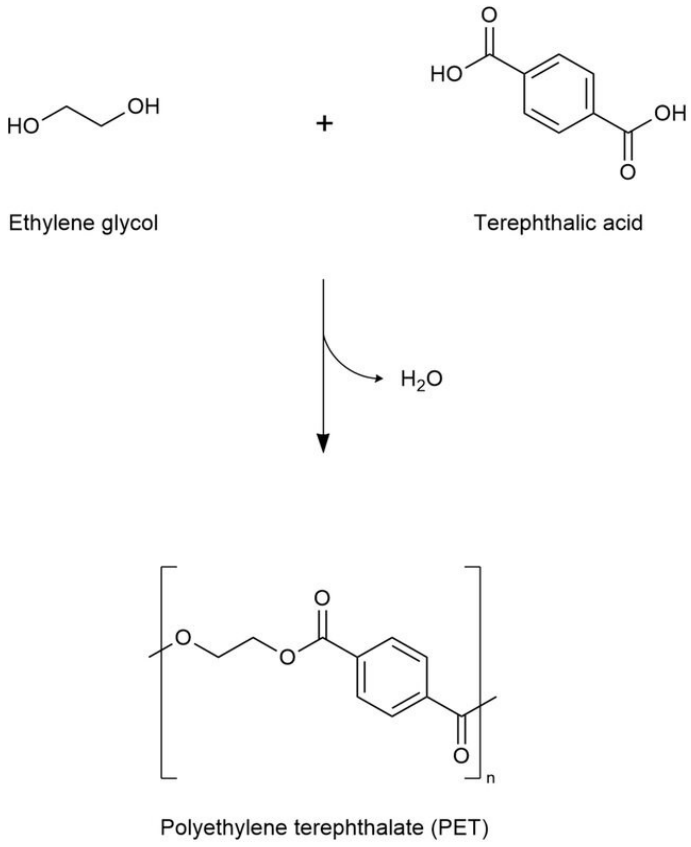

Figure 1: Schematic representation of the chemical synthesis of PET. The polymer is synthesized via polycondensation between TPA and EG, resulting in the formation of long-chain polyester with ester functional groups [10].

Once considered as a beneficial quality, high persistence has now become a major source of environmental contamination. Under natural conditions, PET is not biodegradable and can persist in landfills and natural ecosystems for centuries. Ultraviolet radiation, mechanical forces and specific chemicals lead to degradation into microplastics. During this process, additives, such as pigments and stabilizers, may be released into the environment, potentially exacerbating environmental harm. Therefore, the consumption of food and water contaminated with PET particles represents a high risk to human health [5].

The presence of MNPs in the human body allows them to be taken up by cells via various pathways. Studies have shown that the final pathway is determined by the MNPs' characteristics in terms of size, shape and chemical surface [9] [10] [11]. Typically, MNPs are internalized via endocytosis by being engulfed by the cell membrane and transported into vesicles. The efficiency of the uptake is inversely proportional to the size of the particles, as NPs can also enter the cell by passive diffusion [7]. Furthermore, research has demonstrated that a disrupted intestinal membrane facilitates the transcellular passage of MNPs

through the gut barrier. This indicates that heterogenous MPs are more likely to cause tissue damage and therefore gain easier access [1]. Moreover, MPs/NPs are able to disguise themselves as natural biological particles. To achieve this, the particles adsorb proteins and other biomolecules to form a "corona." The protein corona can influence how the particles interact with cells and potentially facilitate their uptake [6] [14].

1.3 The triggering effects of MNPs at cellular level

Several studies have shown that exposure of plastic particles to human cells can induce oxidative stress. This phenomenon can be attributed to the overproduction of reactive oxygen species (ROS) relative to antioxidants such as vitamin C [15]. Typically, ROS function in the context of cellular signaling and homeostasis. However, imbalance between ROS generation and the antioxidant system can result in damage to cellular components, including lipids, proteins, and DNA. Such consequences may even result in a disruption to cellular function or cell death [16].

1.3.1 ROS – the initial catalyst

ROS are chemically reactive molecules containing oxygen, such as superoxide anions (O_2), hydrogen peroxide (H_2O_2) and hydroxyl radicals (•OH). ROS can be induced by both extracellular and intracellular factors (Figure 2) [17]. Extracellular, ROS production occurs when

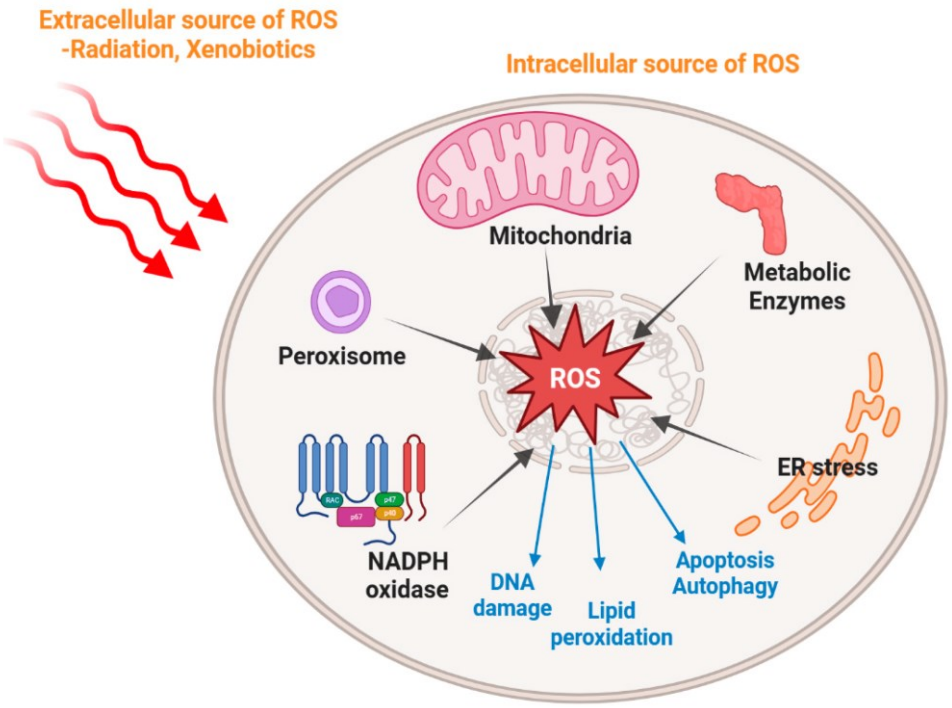

Figure 2: The intra- and extracellular sources of ROS. In addition to mitochondria, organelles such as the endoplasmic reticulum (ER) and peroxisomes can be initiators of ROS. Extracellular, UV-radiation and xenobiotics, including MNPs, promote increased ROS production [17].

plastics are weathered, where environmental conditions such as UV radiation and oxidation alter the plastic's surface, leading to the formation of free radicals. These radicals can react with oxygen, increasing ROS levels once the aged plastics enter cells [18] [19]. Intracellular, ROS are generated when MNPs are internalized by cells through pinocytosis or endocytosis [20]. Once inside, they are recognized as foreign substances, triggering immune responses that activate NADPH oxidase to produce ROS as a defensive mechanism [21]. Smaller particles like NPs are particularly potent in generating ROS because their small size enables easier penetration of cell membranes, thereby increasing their toxicity and ROS production [2].

1.3.2 Mitochondria – the organelle dysfunction

In addition to disrupting the physiological processes of individual cells, MNPs can also affect their organelles, one of which is the mitochondria. This is a major concern, because the mitochondria, the powerhouse of the cell, are the primary site of adenosine triphosphate (ATP) production in cells. Moreover, under physiological conditions mitochondria produce certain amounts of ROS as a result of electron transfer during ATP synthesis. However, exposure to MNPs has the potential to disrupt these essential functions, leading to adverse outcomes [22]. While most MPs are too large to directly enter this organelle, they can nevertheless contribute to mitochondrial damage by increasing in ROS levels in the cytosol, which subsequently affect nearby mitochondria [20]. On the other hand, NPs can more easily penetrate mitochondrial membranes and cause direct damage. This leads to destabilization of the mitochondrial membrane potential, which in turn triggers a cascade of damaging effects (Figure 3). These include further ROS production, loss of ATP generation capacity and, ultimately, the initiation of programmed cell death (apoptosis) [13].

1.3.3 Inflammation – the begin of chronic diseases

This significant increase in ROS generation can additionally induce inflammatory effects by specifically triggering the NF-κB signaling pathway, leading to the production of pro-inflammatory cytokines such as TNF-α, IL-6, and IL-1β. These cytokines reinforce the inflammation by recruiting immune cells to the affected tissues. In response, the immune cells proceed to create ROS [21]. In addition, in the case of mitochondrial damage, they release mitochondrial DNA (mtDNA), signaling danger within the cell. As a response the ongoing cycle of oxidative stress and inflammation continues. Perpetual inflammation can lead to severe tissue damage and consequently be a causing factor for the development of several chronic illnesses [23].

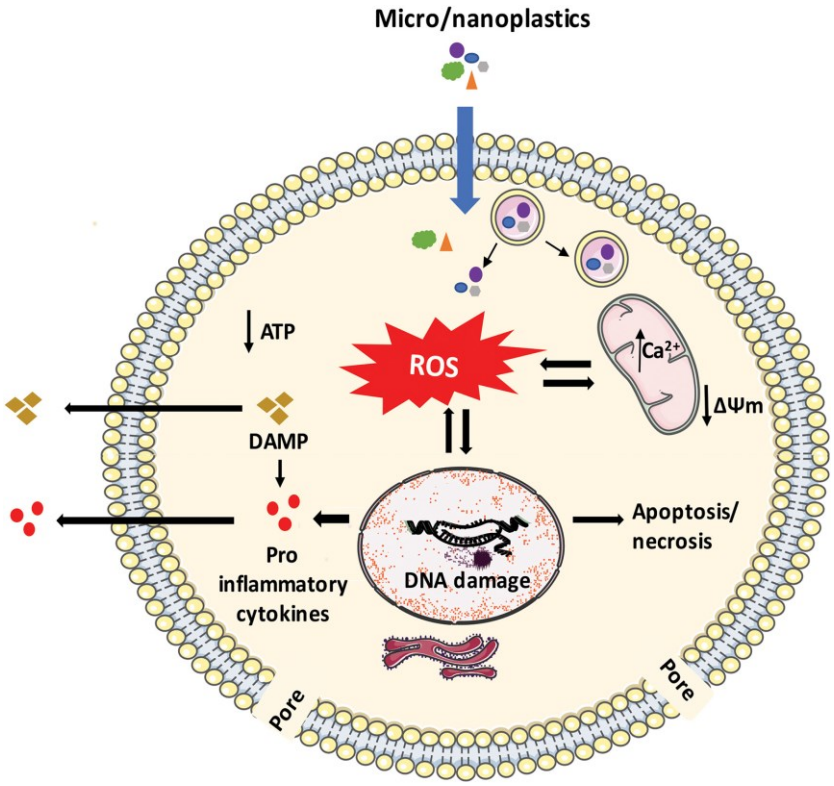

Figure 3: The intracellular toxic effect of MNPs. Exposure to PET-particles initiates a cascade of interconnected cellular responses and triggers the generation of ROS, and further induces mitochondrial ROS. This damage leads to destabilization of the mitochondrial membrane potential, release of mtDNA (depicted as damage associated molecular patterns (DAMP)) and reduced ATP-production. In combination with DNA-damage caused by ROS, pro inflammatory cytokines are induced, leading to inflammatory responses by the cell. Finally, DNA damage cause cell death [13].

1.4 Objective

In view of the substantial scientific evidence already available on the adverse effects of plastic exposure on human health, this study aims to investigate the inflammatory impact of particularly MNPs of PET on human cells. Specifically, the study seeks to compare the effects of different concentrations of these plastic fragments using particles of rather uniform size and irregular shape [24].

Since PET-particles can enter the body through both, the respiratory and digestive tracts, human cell lines representing these pathways were included in the analysis [13]. The primary focus is to evaluate the generation of ROS at both extracellular and intracellular levels, as they are known to activate inflammatory processes. Additionally, knowing the potential cytotoxic effect of ROS this study will include an assessment of cell viability across different concentrations [16] [17]. Lastly, it has been shown that MNPs exert an inhibitory effect on cellular growth [26]. To investigate this effect with PET-particles, spheroids will be used to assess cell growth.

2 Materials and Methods

2.1 Materials

All necessary reagents, chemicals, and assay kits were ordered from commercial suppliers (further details are provided in the description of the method) and, if not otherwise stated, used according to the manufacturer's instructions.

The PET-particles used for these experiments were produced within our project group. The particles were suspended in 0.5% sodium dodecyl sulfate (SDS). The PET stock solution's concentration was 300 µg/ml and for the fluorescein-linked PET-particles (abbreviated as PET-FLUO) 4000 µg/ml. The stock solutions were diluted according to the needs of the experiments. The equivalent diameter (D_{eq}) of the particles was determined using light microscopy (Nikon Eclipse TE2000-S). Both suspensions were pipetted on a microscope slide. Images were taken under the microscope and the diameters calculated using ImageJ software. The calculation of D_{eq} is based on the diameter of spherical bodies, assuming they have similar properties to the used plastic particles [27]. For further determination of size distribution, the intensity-weighted hydrodynamic diameter (Z-average) was calculated with the Dynamic Light Scattering method (DLS) (Malvern Panalytical Zetasizer Pro).

2.2 Cell culture

For the representation of the human colon, the human colon cancer cell line HCT-116 (ATCC CCL-247™, USA) and human colorectal adenocarcinoma cell line HT-29 (ATCC HTB-38™, USA) were used. To make a direct comparison between a healthy and a cancer cell from the same tissue, the mouse embryonic fibroblasts NIH/3T3 (ATCC CRL-1658™, USA) and the human fibrosarcoma cell line HT-1080 (ATCC CCL-121™, USA) were included in the experiments. In addition, a human non-small cell lung cancer cell line H460 (ATCC HTB-177™, USA) was included to extend the study of the effect on other tissues. To ensure the optimal conditions for cell growth each cell line was seeded in a monolayer culture and was incubated at 37 °C and 5% CO_2 in a T75 flask. For the cancer cell lines the Roswell Park Memorial Institute medium (RPMI-1640) was used, while the NIH/3T3 cells were cultured with the Dulbecco's Modified Eagle's Medium (DMEM) – high glucose. Both medias were supplemented with 1% penicillin/streptomycin (P/S), 1% L-glutamine (L-Glu) and 10% fetal bovine serum (FBS). Unless otherwise specified, all the following procedures were performed under the Laminar Air Flow (LAF) to maintain a sterile environment for the to-be treated cells.

2.2.1 Cell splitting

Splitting was performed 2 to 3 times per week to prevent cell overgrowth and nutrient deficiencies. Before splitting the cells, their confluence was checked under the microscope. If it was between 70-80% the cells were split by firstly taking out the medium with a 10 ml serological pipettes. Secondly the cells had to be washed using 3 to 5 ml of Dulbecco's Phosphate buffered Saline (PBS). In the following step 1 to 2 ml of Trypsin (1%) was added to the flask and then incubated for 5 minutes to detach the adherent cells from the flask. The flask was then refilled with medium to a total volume of 13 ml, and the amount of cell suspension added back to the flask was adjusted based on the time until the next experiment, allowing sufficient time for cell regrowth. Approximately every two weeks the flask was replaced by a new one.

2.2.2 Cell counting

The cell number was evaluated by using the cell suspension from the split and diluting it to a ratio of 1:10, i.e. 10 µl of the cells were mixed with 90 µl of PBS. After resuspension, 10 µl of the dilution was carefully pipetted onto a Neubauer chamber. To ensure equal cell distribution, the pipette tip was placed at the edge between the coverslip and the chamber. By slowly dispensing the dilution, the formation of air bubbles was prevented, and capillary action enabled an even distribution of the cells across the counting grid. Each of the four major quadrants was divided into 16 smaller quadrants to facilitate the counting. The cells were counted from left to right and then in the next row from right to left and so on. In cases where cells are placed directly on the quadrant outline, only two sides can be included in

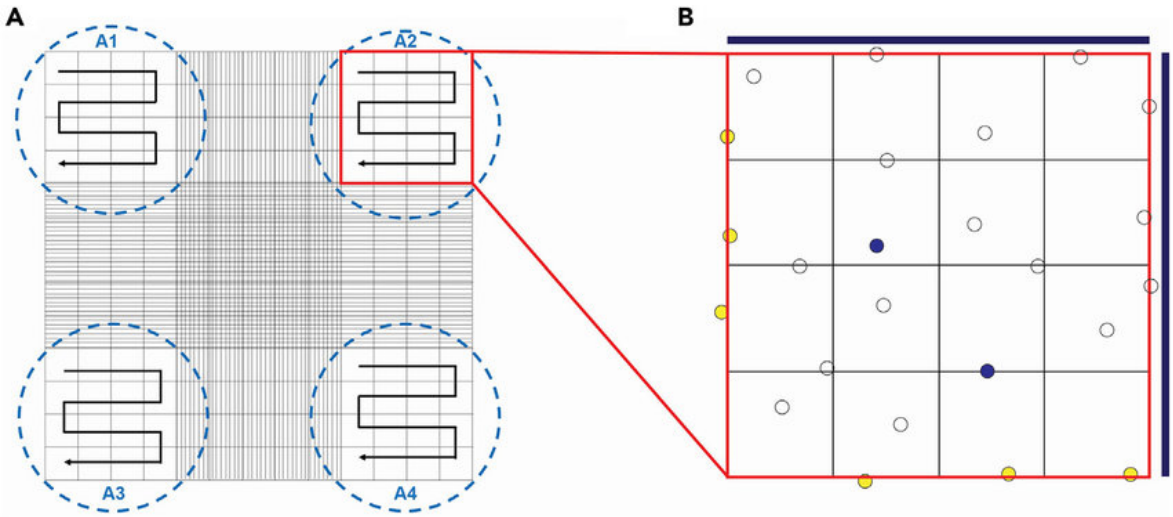

Figure 4: Illustration of cell counting with the Neubauer chamber. (A) depicts the full grid viewed under the microscope, illustrating the order in which cells are counted. (B) shows an enlarged view of one of the four quadrants, demonstrating that only cells touching two of the designated outlines are included in the final calculation [28].

the counting process (Figure 4) [28]. This process is being repeated for each of the four large quadrants. Finally, the sum of the cells was divided by 4, multiplied by 10000 and the dilution factor. The result provides the mean number of cells per milliliter.

2.3 Cell viability

The MTT-assay was utilized to assess cell viability in the HCT-116 and H460 cell lines. This assay is a well-established colorimetric measurement, which is based on the metabolic reduction of the yellow tetrazolium salt MTT [3-(4,5-dimethylthiazol-2-yl)-2,5-diphenyltetrazolium bromide] to purple colored formazan crystals [29]. This conversion is initiated by reducing agents produced in viable cells. The cells are lysed using a dimethyl sulfoxide (DMSO) solution, which dissolves the formazan crystals. The detected absorbance of the solution is directly proportional to the number of viable cells present [30].

The cells were seeded with a concentration of 2 x 10^4 cells/ml in a transparent 96-well plate and incubated for 24 hours at 37 °C on the first day. A stock solution of 20 µg/ml was prepared for the PET suspensions. Half of the stock solution was mixed with the same amount of media to create a 10 µg/ml solution (1:1 dilution). This step was repeated for all the needed concentrations (0.31 – 5 µg/ml) by always taking the solution of the previous made concentration. For this assay the fluorescence labelled PET-particles and regular PET were included. After treatment, the plates were incubated for 72 hours. On the last day, the media was removed, and cells were treated with 100 µl of the MTT-mixture. This mixture was prepared in a Petri dish by mixing the MTT-solution (250 mg Thiazolylblautetrazoniumbromid in PBS (MTT, Merck, St. Louis, Missouri, USA)) with supplement free medium in a ratio of 1:7. After 4 hours of incubation the plate was carefully emptied with a multichannel pipette and 100 µl of DMSO was added to each well. Additionally, DMSO was also pipetted to a row of empty wells. The absorption was detected with the Tecan Infinite M200 Pro (Männerdorf, Switzerland) and iControl Software at 550 nm (measurement wavelength), while the reference wavelength was at 690 nm.

2.4 Detection of total ROS

For the detection of the total ROS level the Total Reactive Oxygen Species Assay Kit 520 nm (Invitrogen™, Thermo Fisher Scientific) was used, and all cell lines were included. Inside the cells, the included fluorogenic dye 2',7'-dichlorofluorescin diacetate (DCFDA) is first conversed to dichlorodihydrofluorescein (DCFH). Then the compound becomes fluorescent by being oxidized to DCF in the presence of ROS. The cells' fluorescence intensity is being detected and is directly proportional to the ROS level in the cells [31] [32].

On the first day, the cells were seeded in a flat black or white 96-well plate with a concentration of 2 x 10^3 cells per well and incubated at 37 °C for 24 hours. The following day the ROS stain was prepared by adding 40 µl of DMSO to the vial of the 500X ROS assay stain stock solution and mixing it well. The media was removed, and the stain added in a final concentration of 0.4 µl/ml. After 1 hour of incubation the cells were treated with PET-suspensions, as described at the MTT-assay. To avoid an interference with the detection of fluorescence intensity by DCF, only PET and RPMI-1640 media without phenol red were used. As a positive control H_2O_2 was used. The fluorescence intensity was immediately measured at 488/520 nm using the Tecan reader. After 2 hours of incubation at 37 °C, the measurement was repeated.

2.5 Assessing mitochondrial ROS

The MitoSOX™ Red Assay (Invitrogen™, Thermo Fisher) is based on a fluorogenic dye, that can specifically detect ROS produced by the mitochondria. The triphenylphosphonium (TPP)-linked hydroethidine derivative is proven to form 2-hydroxy-mito-ethidium (2-OH-Mito-E+), a fluorescence product, through a reaction with ROS [33]. The TTP moiety is a lipophilic cation and therefore attracted to the negatively charged mitochondrial membrane. Due to its high lipophilicity, it passes the mitochondrial membrane and remains there due to the maintenance of the electrochemical gradient [33] [34]. For this reason, the results can be specifically assigned to the mitochondria.

The assay was executed as suggested in the protocol by the producer. First, the 50 µg red staining solution MitoSOX™ Red was dissolved in 13 µl of DMSO to create a 5 mM stock solution. The cells were prepared for staining by seeding 1 x 10^4 cells per well in a black 96- well plate on the first day. After 24 hours of incubation at 37 °C, the media was removed with a multichannel pipette. After that the PET-concentrations (produced as described at the ROS assay) from 0.31 µg/ml to 5 µg/ml were added to the adherent cells in the wells. As a positive control 30% H_2O_2 was used. The cells were incubated for one hour and in the meantime the staining stock solution was diluted with PBS to a 5 µM solution. 100 µl of this solution was added to the wells and incubated at room temperature under the protection of light using aluminum foil. During incubating, the plate was placed on a shaker to ensure an even staining of the cells. After 20 minutes, the staining solution was removed and the cells were washed by adding PBS, waiting 5 minutes and then removing the PBS. These steps were repeated twice. Finally, 100 µl of PBS was added to each well and then detected with the Tecan reader at 488/580 nm. Furthermore, the cells were observed under a fluorescence microscope (Nikon Eclipse TE2000-S).

2.6 Cell proliferation

In comparison to two-dimensional cultures, three-dimensional (3D) spheroids offer a more accurate representation of in vivo tissues. By allowing the cells to adopt their natural morphology and not to adhere flat to the surface of a plate, cells replicate the physiological tissue microenvironment, making them more applicable for studying real-life biological processes [37] [38].

Two stock solutions were prepared for each cell line, using the HT-29 and HT-1080 cells at a concentration of 2 x 10^4 cells per ml. For the PET-treatment, PET-FLUO were directly added to one stock solution of each cell line at a concentration of 2 µg/ml. Prior to use, the 96-well round-bottom plates were coated with an 1% (m/V) agarose in water solution to prevent cell adhesion to the bottom surface. For preparation, 2-Hydroxyethyl agarose (Sigma-Aldrich Corporation) and deionized water (LaboStar PRO water system, Evoqua Water Technologies GmbH) were combined in a falcon tube and heated in a water bath at 80-90 °C. Once the agarose had fully dissolved, 10 ml of the solution were transferred to a Petri dish. A thin coating without air bubbles was achieved by using a multichannel pipette, with 100 µl added to each well and immediately removed again. These steps were repeated for every row. The plates were cooled at room temperature and stored in the fridge at 4 °C.

On the first day of the experiment, 100 µl of the stock solutions (with and without PET-FLUO) were added to each well of the agarose coated plate to provide a direct comparison from their initial seeding. The plate was then incubated for a period of 48 hours. On the third day, images were captured using the fluorescence microscope. This process was repeated on the fourth, sixth, and seventh day. Subsequently, the images were then analyzed using ImageJ to calculate the area of the spheroids.

2.7 Statistics

In all experiments, unless otherwise stated, each concentration was at least triplicated and the experiments repeated three times. In every run, an untreated control without particles was included as a reference. Furthermore, for the detection of general and mitochondrial ROS the experiments were executed with a positive control to guarantee reliability and validity of the results. The data was analyzed using Microsoft Excel and all the values are presented as mean ± standard deviation (SD). The results were statistically analyzed using a t-test and a difference of $p < 0.05$ was considered statistically significant.

3 Results

3.1 MNP's characteristics

To get a better understanding of the particles dimension and distribution in the PET-samples, the characterization of PET and PET-FLUO was performed with two methods. The size of the particles was determined by calculating their D_{eq} with the ImageJ software, while the DLS method provided more information for the homogeneity or rather heterogeneity of the suspensions. The Z-average represented the mean diameter of the particles, characterized by the DLS method, while a high dispersity value indicated a broad range of particle sizes in the sample.

The results (Table 1) demonstrated a comparable mean D_{eq} between the two samples. The high standard deviation of PET-FLUO (SD = 0.97 µm) implied a broader range of particle sizes in the suspension, compared to PET (SD = 0.52 µm). The proximity of the median to the mean of PET indicated a symmetrical distribution of the PET-particles. In contrast, the D_{eq}-median of PET-FLUO was noticeably lower than the mean size of the particles. In combination with the SD, it indicated a broad range of particle sizes in the sample. Nevertheless, a high number of particles are below 0.94 µm.

A comparison of the Z-average between the samples demonstrated that the PET-sample (0.96 ± 0.098 µm) contains a larger number of smaller sized particles to PET-FLUO (1.7 ± 0.26 µm). Moreover, PET had a lower dispersity, indicating that the sample predominantly consisted of uniformed-sized particles. In contrast, PET-FLUO exhibited a high dispersity of 0.55, confirming a polydisperse suspension. Overall, both samples exhibited a range of sizes, which is consistent with natural observations of plastic debris.

	c [µg/ml]	D_{eq} [µm]	D_{eq} - median [µm]	Z-average [µm]	Dispersity
PET	300	1.24 ± 0.52	1.23	0.96 ± 0.098	0.17
PET-FLUO	4 000	1.25 ± 0.97	0.94	1.7 ± 0.26	0.55

Table 1: Characteristics of PET and PET-FLUO. The characterization of the mean size and size distribution was performed with light microscopy/ImageJ and with DLS. Both samples show a variation in particle size, while the PET-FLUO-sample demonstrates a high Z-average, indicating a high presence of large particles. c: concentration of the stock solutions; D_{eq} represents the mean size of the particles ± SD; D_{eq}-median: 50% of the particle's sizes are above and below this value. Z-average: represents the mean diameter of particles, presented as mean ± SD. Dispersity: value for the particle size distribution, an increase in value indicates a higher degree of polydispersity

3.2 The effect of PET-MNPs on cell viability

The cell viability was assessed using the MTT-Assay to determine the concentration at which PET exhibits inhibitory effects on cell viability. For this experiment both PET-samples were administered in a concentration range of 0 to 5 µg/ml to HCT-116 and H460 cell lines. The measured absorbance directly reflects the metabolic activity of the cells.

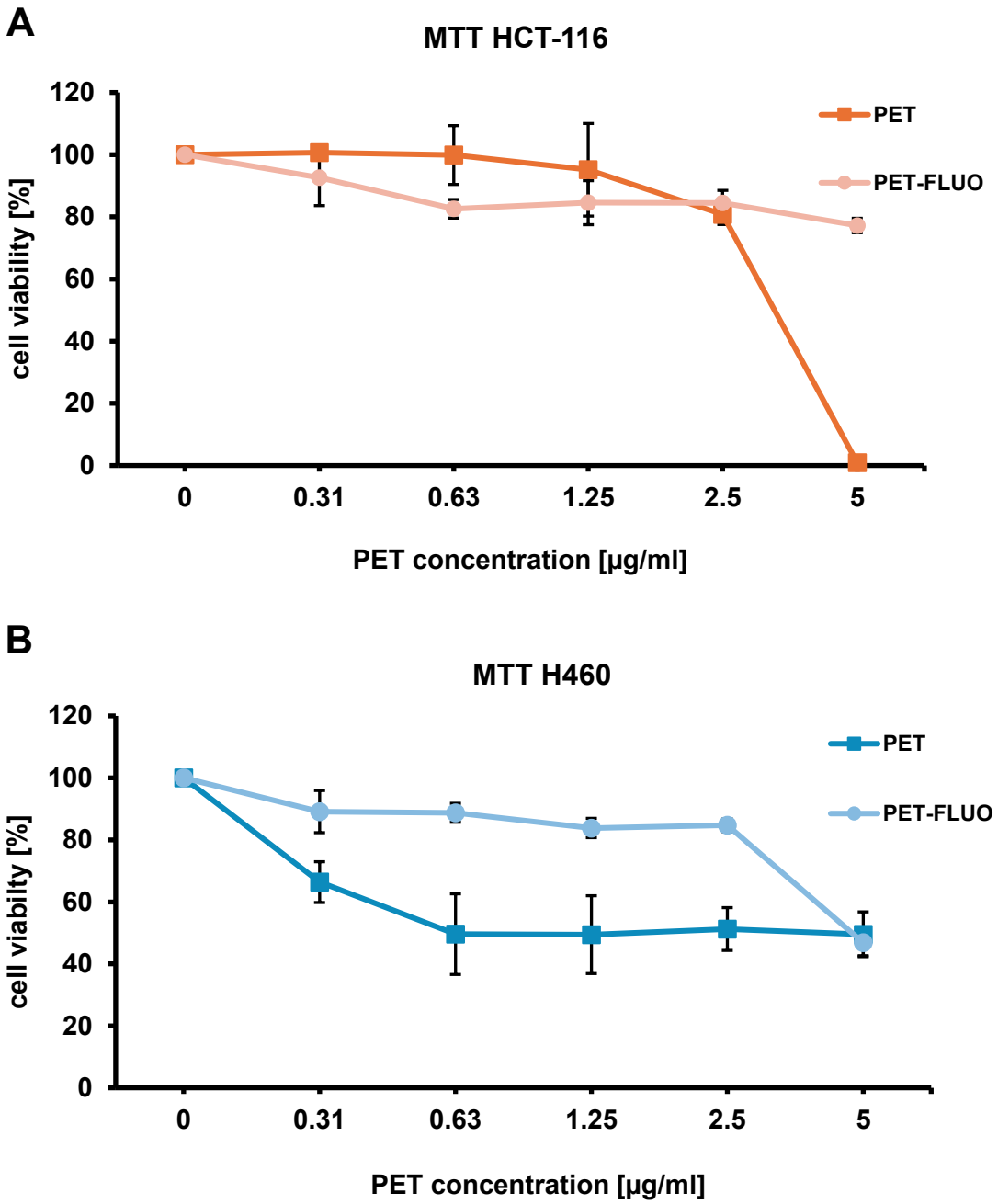

Figure 5: The cell viability of HCT-116 (A) and H460 (B) cells. The darker colored line represents the PET- particles, while the lighter one corresponds to the PET-FLUO particles. The results were normalized to a control (untreated cells). Data are presented as mean ± SD, with n=3 replicates.

The HCT-116 cells exhibited generally a concentration-dependent decrease in cell viability when exposed to both PET-samples (Figure 5A). At lower concentrations ranging from 0 to 2.5 µg/ml, cell viability remained above 80%. PET-particles lead at a concentration of 5 µg/ml to a nearly completely loss of cell viability, indicating cytotoxicity. In contrast, PET-FLUO particles demonstrated a comparatively lower toxic effect, with a maximum loss of maximum 20% of viable cells.

Exposure to PET-particles also led to a consistent decrease in cell viability in H460 cells (Figure 5B). At all tested concentrations PET-FLUO is more toxic than PET with observed differences in cell viability ranging from 20 to 40%. Similar to HCT-116 cells, PET induced a rapid increase in cell viability inhibition from the concentration of 2.5 µg/ml. Nevertheless, at 5 µg/ml both PET-samples show an equivalent effect.

Overall, a comparison of the two cell lines revealed that the effects of the two PET-samples resulted in different inhibitor effects on cell viability. In general, H460 cells appeared to be more sensitive to the exposure of both PET-samples compared to HCT-116 cells. Additionally, PET had a more detrimental impact on cell viability than PET-FLUO. In contrast, HCT-116 cells' viability exhibited no difference compared to the untreated cells' once when exposed to PET, whereas PET-FLUO caused a loss of viable cells at a maximum of 20%. The toxic effect of the PET-particles became apparent only at a concentration of 2.5 µg/ml, ultimately leading to a percentage of 0.01% of viable cells at the highest concentration.

3.3 Determining the total ROS level

To verify whether PET particles induce oxidative stress in the cell lines, ROS levels were measured by exposing the cells to the range of concentrations from 0.3 to 5 µg/ml of the PET-particles. The ROS levels were directly quantified using a plate reader measuring fluorescence intensity after the addition of DCFDA, a compound, which fluoresces upon encountering ROS. H_2O_2 was determined as the positive control for this assay.

The evaluated data indicates that after 10 minutes of incubation with PET, all cell lines produced ROS (Figure 6). In particular, at higher concentrations of PET (2.5 and 5 µg/ml) the increasing PET-concentrations led to statistically significant increases in ROS generation across all cell lines. At the first measurement time, HT-1080 cells demonstrated the highest effect at PET-exposure of 5 µg/ml, followed by HCT-116 and H460 (Figure 6A). NIH/3T3 showed a relatively low response to the treatment, even at the highest exposure. At the lower concentrations 0.31-1.25 µg/ml the production of ROS was only slightly higher compared to the control group. In contrast, H_2O_2 induces higher ROS generation compared to the highest concentration of certain cell lines, such as HCT-116, H460, and HT-29 (Figure 6B). Noticeably, the ROS generation in HT-1080 cells was higher at 5 µg/ml than when

exposed to H_2O_2. Moreover, H460 cells showed almost the same ROS level with PET at the highest concentration as with the positive control.

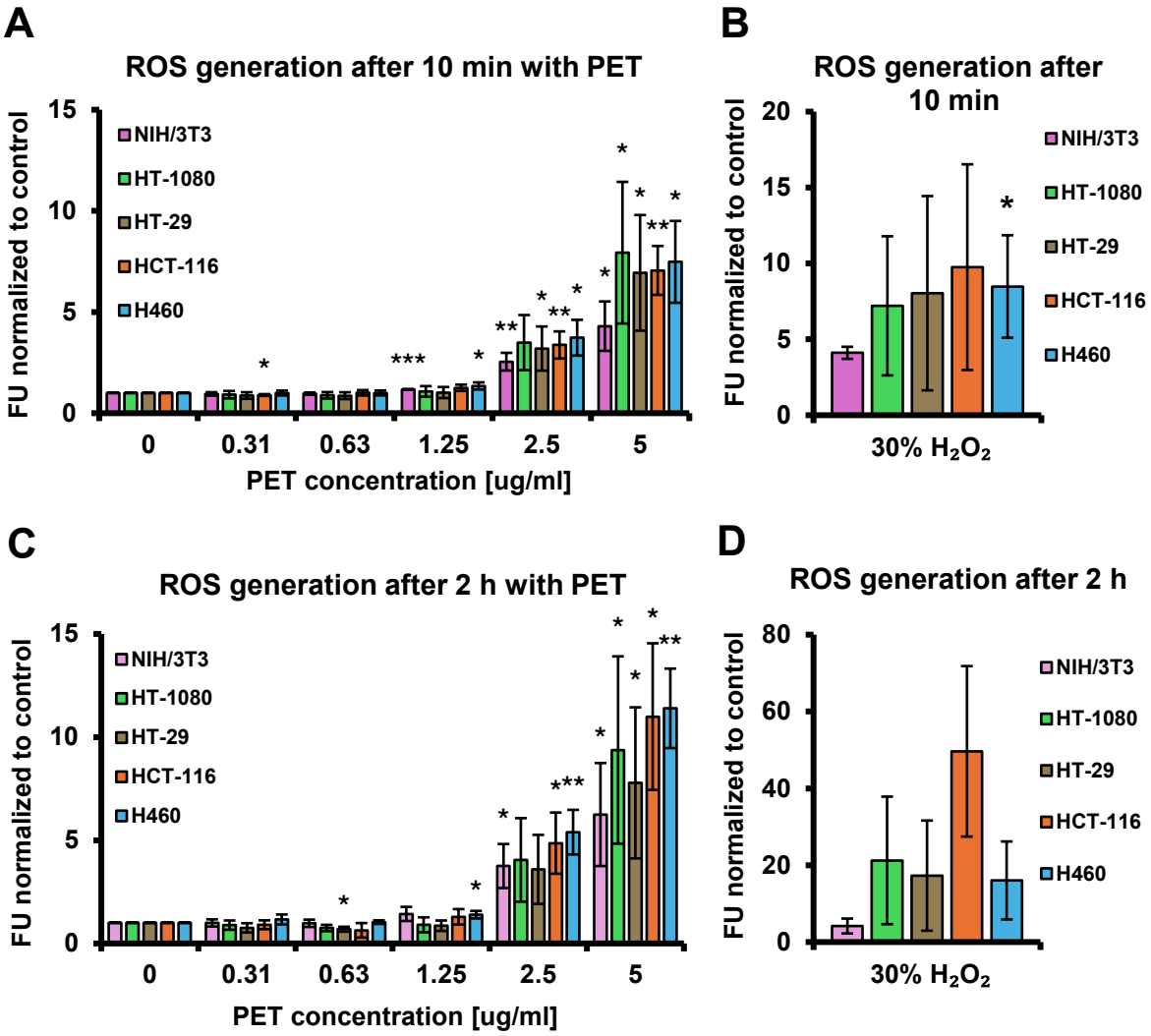

Figure 6: ROS Assay results for all cell lines at 10 minutes (A, B) and after 2 hours (C, D) of exposure. The x-axis represents the concentrations of the exposed PET-MNPs, and the y-axis depicts the fluorescence units (FU) normalized to the control (untreated cells). The data are presented as mean ± SD, with n=3. Statistical significance was calculated using Microsoft Excel, with * < 0,05; ** <0,01; *** <0,001.

After 2 hours of incubation the ROS levels increased at the two highest concentrations, while no noticeable difference between the two measurement points was observed at the lower concentrations (Figure 6C). Moreover, ROS level of H460 and HCT-116 cells exceeded the one of HT-1080 cell line. NIH/3T3 exhibited the highest resistance to the exposure of PET, producing less ROS than any other cell line. Notably, the observed increase in ROS remained statistically significant at the highest concentrations (2.5-5 µg/ml), even after two hours of exposure.

3.4 Mitochondrial ROS

The mtROS represented a key area of interest, aiming to determine whether PET causes stress reactions within mitochondria. After treatment with PET-particles, the cells were incubated with a fluorogenic dye to detect the fluorescence intensity as a direct representation of the amount of mitochondrial ROS.

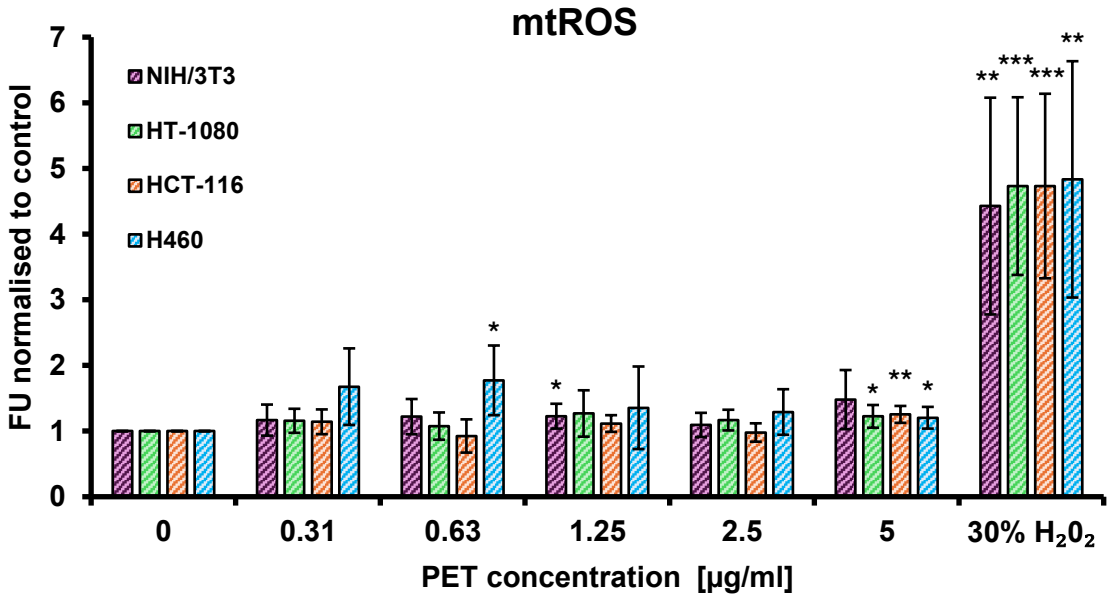

Figure 7: The results of mtROS across all cell lines following PET exposure. The x-axis represents the concentrations of PET-particles, while the y-axis depicts FU normalized to the control group. The data are presented as mean ± SD, with n=3. The significance was calculated with Microsoft Excel. * < 0,05; ** <0,01; *** <0,001.

Figure 7 shows that the level of mtROS observed were relatively similar to those in cells without treatment, indicating that mtROS was predominantly absent. In contrast, the treatment with H_2O_2 led to a significant increase in ROS levels, confirming the reliability of the assay. Despite the increase in PET concentration, no proportional increase in mtROS was observed. Specifically, H460 cells had a statistically significant higher ROS generation at 0.63 µg/ml than at 5 µg/ml, presenting the highest levels across all cell lines and PET concentrations. At a concentration of 5 µg/ml, all cancer cell lines exhibited a significant elevation in ROS levels compared to untreated cells, whereas NIH/3T3 exhibited no significant change of ROS generation. Notably, NIH/3T3 cells only demonstrated a significant increase at 1.25 µg/ml of PET-exposure. Overall, in comparison to the results of the total ROS, this assay demonstrated no dose-dependent increase in mtROS.

Under the fluorescence microscope, stained mitochondria were distinctly visible, particularly at the higher concentrations. In Figure 8, NIH/3T3 cells are shown, treated with PET ranging from 0.63 µg/ml to 5 µg/ml , including the control groups. It is evident that the control group showed no fluorescence, whereas the H_2O_2 treated group displayed the most intense red fluorscence, serving as a positive control. At the highest concentration the multiple mitochondria were clearly visible, indicating the presence of high mitochondrial ROS levels.

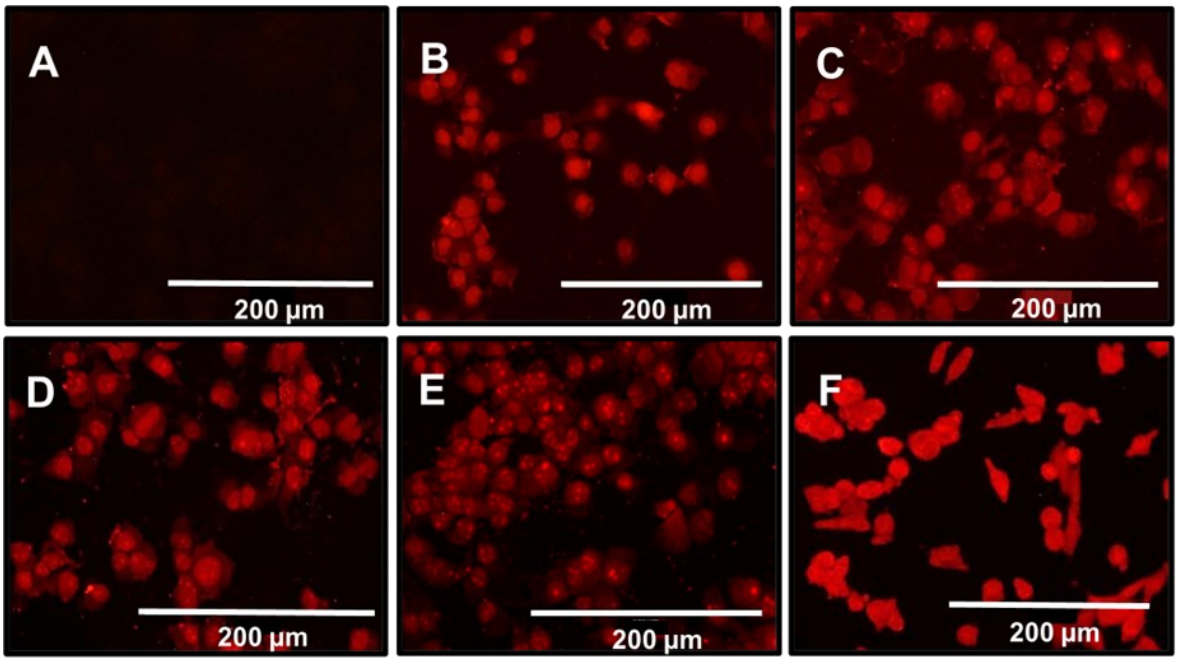

Figure 8: Fluorescence microscopy images of NIH/3T3 microscope exposed to different PET-concentrations. The pictures represent the following exposure: (A) 0 µg/ml (control group); (B) 0.63 µg/ml; (C) 1.25 µg/ml; (D) 2.5 µg/ml; (E) 5 µg/ml; (F) H_2O_2. Scale bars: 200 µm

3.5 Effect on cell growth on a 3D model

Spheroids were created to determine the inhibitory effect of PET-FLUO on cellular proliferation. The cells were combined with PET-FLUO at a concentration of 2 µg/ml and seeded on an agarose-coated 96-well plate to prevent cell adhesion to the bottom surface. For comparison, cells without treatment were prepared the same way. The spheroids' growth process was captured from day 3 to 7 under a fluorescence microscope and the area calculated with ImageJ.

Figure 9 presents the growth of HT-29 spheroids treated with PET-FLUO compared to the untreated control group. Both groups started with comparable size on day 3, serving as the baseline for subsequent measurements. The spheroid populations showed a consistent increase in growth. Nevertheless, no significant size differences were observed.

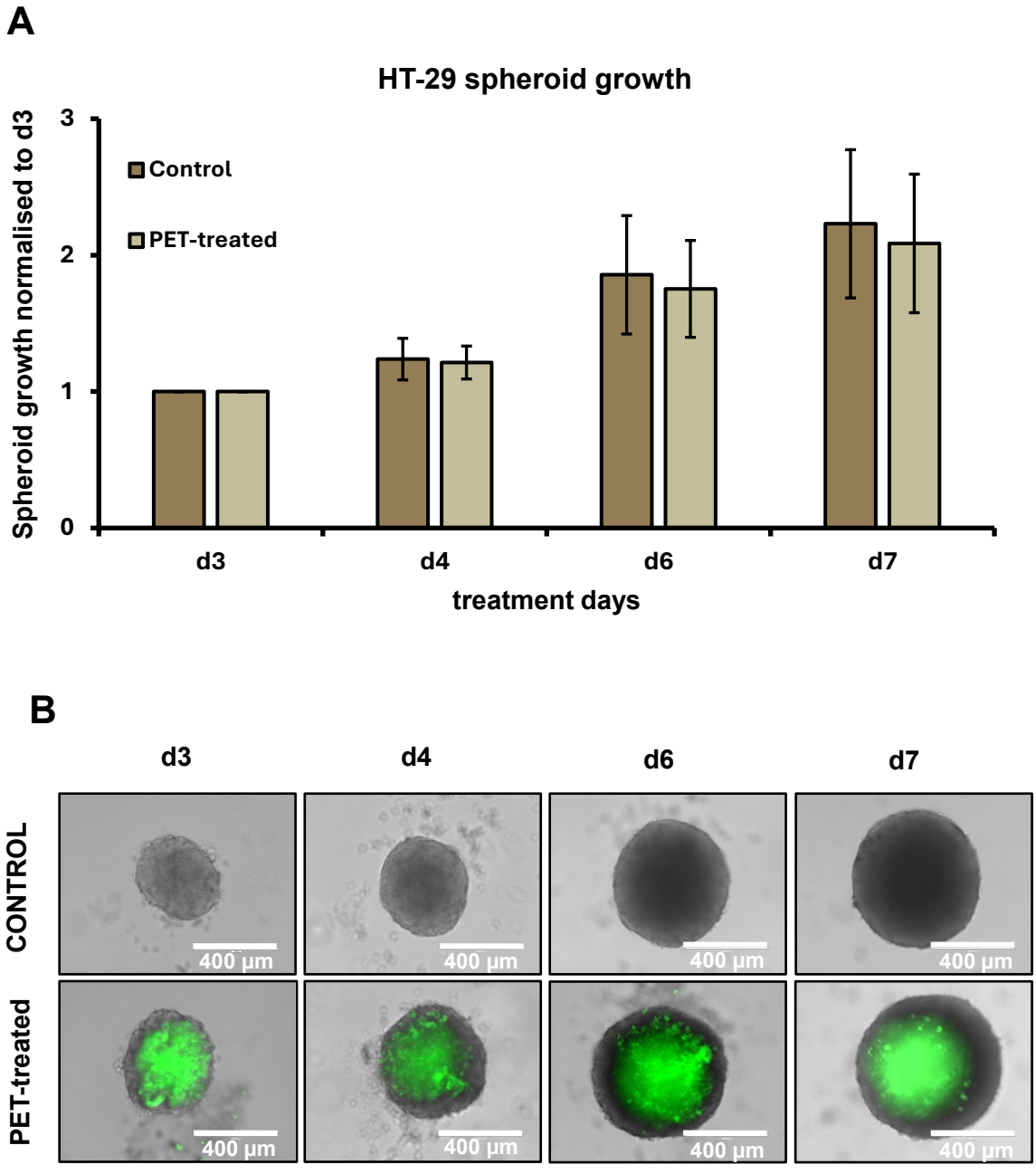

Figure 9: The growth of HT-29 spheroids with and without PET-treatment over 7 days. The spheroids were treated with 2 µg/ml PET-FLUO. (A) shows the calculated areas of the spheroids normalized to day 3, with data represented in mean ± SD, n=3. (B) illustrates the photographic documentation of the spheroid growth, where the distribution of the fluorescently labeled PET-particles can be clearly observed. The area was calculated with ImageJ. Scale bars: 400 µm

Figure 10B illustrates, that the distribution of PET-FLUO became increasingly centralized to the necrotic core of the spheroid with the passage of time. While the distribution at day 3 to day 6 remains largely unaltered, at day 7 the particles are noticeable more concentrated in

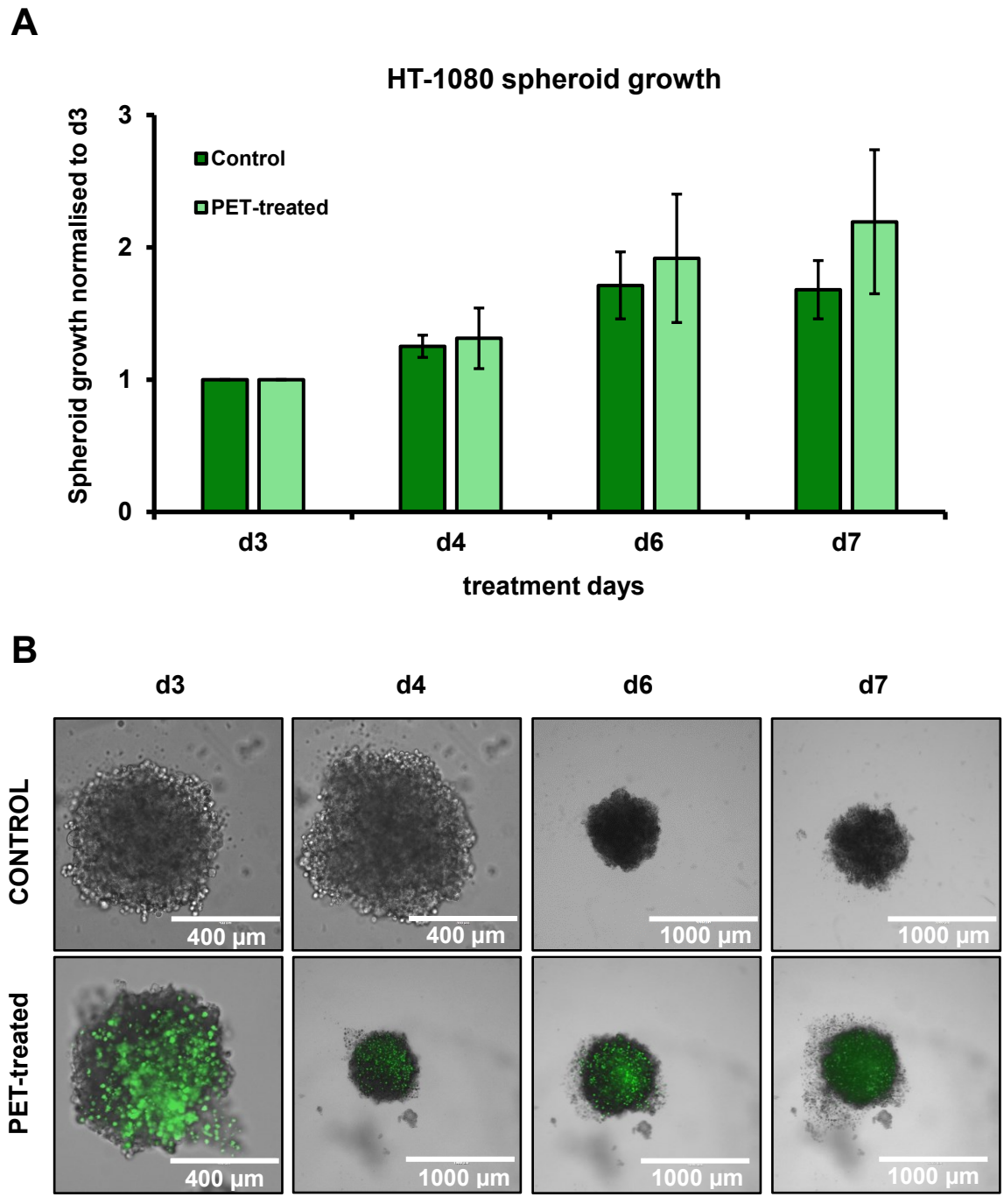

Figure 10: The growth of HT-1080 spheroids with and without PET treatment over 7 days. The spheroids were treated with 2 µg/ml PET-FLUO. (A) shows the spheroid growth normalized to day 3. The results are shown in mean ± SD, n=3. (B) illustrates the photographic documentation of the spheroid growth and demonstrates the PET-particle distribution. Scale bars for control d3/4: 400 µm; for d6/7: 1000 µm; for PET-treated: d3: 400 µm; d4/6/7: 1000 µm

the central region of the spheroid. In contrast, HT-1080 spheroids showed a consistent distribution pattern throughout the treatment period (Figure 10B).

The HT-1080 cells demonstrated a comparable growing pattern to that of HT-29 cells. The control group as well as the treated group showed an increase in growth, although the control group showed no progress over the last two days. Unlike HT-29, the HT-1080 cells consistently maintained a larger size compared to the untreated cells throughout the observation period. Nevertheless, the overlap in variability between the two groups indicates that there is no inhibitory growth effect resulting from PET-FLUO.

4 Discussion

The aim of this study was to determine if PET-MNPs have the potential to induce pro-inflammatory effects on different cell lines *in vitro*, with focus on the total and mitochondrial ROS generation. The findings of the individual experiments suggest that a potential pro-inflammatory effect by PET-MNPs exists, yet it must be regarded for each specific tissue, as the results showed that each cell line reacted differently to PET-exposure.

The MTT-assay showed a proportional decrease in cell viability following an exposure to higher concentrations, leading even to a loss of 99.9 % in viable cells in the colon cell line HCT-116 at 5 µg/ml. The observed dose-dependent decrease in cell viability in the HCT-116 cell line is consistent with the findings of a previous study, which studied the effects of PS-MNPs [38]. Nevertheless, a noticeable discrepancy between the inhibitory effect of the PET-samples as well as between the tissues was observed. In comparison to PET-FLUO, PET demonstrated a comparatively stronger inhibitory effect on cell viability, which was particularly evident in the H460 cell line. The discrepancy reached a maximum of 40% in terms of viability. The different effects may be attributed to variations in particle size, as the DLS method indicated that PET-FLUO (1.7 µm) contains a significant portion of larger particles compared to PET (0.96 µm). The linking of the particles with fluorescein may led to increased aggregation, explaining the broader range of particle sizes compared to the PET-sample. As documented in previous studies, smaller particles, especially NPs, induce more toxic events than larger ones [13]. Consequently, a difference in the outcome of the MTT-assay can be ascribed to e.g. the variations in particle size.

Excluding the effect at 5 µg/ml, colon cancer cells demonstrated a greater resilience to PET, whereas lung cells exhibited a higher sensitivity. This variation in response emphasizes the necessity of considering the tissue of origin when evaluating the cytotoxic effects of PET, given that different tissues have evolved specific defense mechanisms that are adapted to their typical environmental exposures. Taking the statistically significant high ROS levels in consideration, the total loss of viable cells at the highest exposure could be a result of induced apoptosis [39] [40]. Further experiments would be required to prove this hypothesis. It must be noted that the duration of exposure to PET is not comparable between the two experiments. While the MTT-assay involved contact with the plastic particles for several days, the ROS assay was conducted over a considerably shorter period (2 hours).

As already established in recent findings, this study provided further evidence that microscopic plastic particles cause a dose-dependent ROS generation in a monolayer culture [2] [9] [15]. Especially at higher concentrations, a statistically significant rise in ROS levels across all cell lines was detectable. Following a relatively short period of incubation with

PET-particles, the cells already exhibited significant elevated ROS levels compared to the untreated cells. The data implied that extended exposure to specific concentrations may lead to elevated ROS production.

As already discussed in context of the MTT-assay, the pronounced difference in sensitivity to PET exposure between the cell lines was evident again. Especially, HCT-116 cells showed high sensitivity to PET exposure, while NIH/3T3 demonstrated the lowest levels. This may be a result of the different behavior between cancerous and healthy cell lines towards external factors. Healthy cells typically maintain lower ROS levels compared to cancer cells, because they express higher levels of antioxidants that help regulate oxidative stress more effectively [41]. The results confirmed that PET-particles act as a catalyst of oxidative stress and in further steps potentially damage the cells' viability. For ROS detection, only PET could be included, given that the labelling of the particles with fluorescein interfere with the detected fluorescence intensity from the ROS assays [42].

Interestingly, the mtROS levels did not increase proportionally with higher PET doses. The results showed that the mtROS generation was only statistically significant at the highest concentration for all cancer cell lines. These results indicate that ROS generation cannot be tracked down to mitochondrial ROS but may be formed with the involvement of other cell organelles, such as the endoplasmic reticulum (ER) or peroxisomes, as discussed in the introduction (Figure 2). For further studies, all cell organelles linked to the generation of ROS should be considered.

However, there was an obvious discrepancy between measuring mitochondrial ROS via the plate reader and by fluorescence microscopy. The positive mitochondrial ROS formation as detected by fluorescence microscope, lead to the conclusion that there may be some methodological obstacles in attempting to capture the mitochondrial ROS with the plate reader. The cells frequently detached rapidly from the surface, making it difficult to locate the fluorescence. This may be due to the staining, although the concentration suggested by the manufacturer was used. Fixing the cells for microscopic purposes would prevent the detachment of cells. Moreover, the supplier recommended a staining time of 10-30 min. The 20-minute waiting time proved to deliver the best results, so it was used for the assay. Another potential issue could be the washing steps, which altered the appearance of the cells compared to the live control. This suggests that the current assay may not be fully suitable for plate reader analysis. However, microscopy demonstrated an effect, indicating that the assay requires further optimization to reliably demonstrate this effect in the plate reader.

The investigation on the inhibitory effect of PET-particles on spheroids revealed no evidence of such an effect. This contradicts the results of the MTT-assay, which demonstrated an

inhibitory effect on cell proliferation when exposed to PET-FLUO. This discrepancy may be a result of the different cell accessibility between the 2D and 3D method. The spheroid structure does not allow particles to easily gain access to the individual cells, whereas in a monolayer culture the cell membranes and their receptors are more accessible [43]. The results showed that the particle distribution at the HT-29 spheroids was more concentrated to the necrotic core, showing a more centered distribution. Consequently, not all cells were able to interact with the exposed particles. Moreover, the method presented some limitations. A structural loss was observed of the spheroids with lose cells surrounding the HT-1080 spheroids. The effect was seen in treated and untreated spheroids, implying that the instability is due to the tissue and is not caused by PET. In comparison, the HT-29 spheroids exhibited no structural loss, thereby suggesting that the spheroid's stability is dependent on the cell line.

The results of this research indicate that all pathways associated with ROS generation should be further investigated, given the lack of effects observed in mitochondrial ROS. One possible factor is the role of NADPH oxidase, which has been previously associated with ROS generation in studies investigating the activation following exposure to PS-MNPs [44] [45]. In this case, further investigation is required to establish the exact cellular mechanism by which oxidative stress leads to the activation of inflammation processes. As shown in the study by Woo *et al.*, inflammatory markers, such as TNF-α, should be assessed, as their detection could provide insight into the activation of NF-κB by ROS, further elucidating the inflammatory response mechanisms involved [22].

Given the multiplicity of factors that are crucial for the effect of PET on human cells, further research should also include the characterization of surface charge and shape. As stated in previous studies, the modified surface charge may influence the uptake and distribution of the PET-particles [46] [47]. He *et al.* validated this hypothesis in their investigation of PS-particles, demonstrating that alterations to the plastic’s surface leads to varying degrees in cytotoxicity in hepatic cells [48]. Moreover, the exact shape of the particles should be determined, considering that irregular shaped particles have been proven to induce stronger responses [49]. Therefore, a more comprehensive analysis of the particle characteristics is essential for future research, to elucidate their roles in cellular interactions.

5 Conclusion

The collected data demonstrate that PET-MNPs exert a dose-dependent effect on both cell viability and the generation of ROS, with different sensitivity pattern observed across the cell lines. The MTT-assay revealed a general sensitivity difference between HCT-116 and H460, with stronger cell viability inhibitory effects on H460 cells. The results of this study must be viewed with caution due to the differences in size between the PET-samples, as the particle size is a crucial factor influencing the subsequent cell uptake.

Although this study has demonstrated that in vitro PET-plastic leads to oxidative stress, further studies are necessary to disclose the exact mechanism underlying ROS production. The investigation of mitochondrial ROS showed no substantial difference between treated and untreated cells, indicating that the elevated total ROS levels are caused by other cell organelles. Moreover, no inhibitory effect on cell growth was observed when treated with PET-particles in a 3D model.

The present study forms the basis for a more detailed investigation of the various pathways of ROS generation. Furthermore, the correlation between oxidative stress, inflammation, and potential downstream effects on cell function and tissue integrity remains an important area for further investigation.

Index of abbreviations

2D: two dimensional

3D: three dimensional

ATP: Adenosin triphosphate

DAMP: damaged-associated molecular pattern

DCF: dichlorofluorescein

DCFDA: 2',7'-dichlorofluorescin diacetate

DCFH: dichlorodihydrofluorescein

D_{eq}: equivalent diameter

DMEM: Dulbecco's Modified Eagle's Medium

DMSO: Dimethyl sulfoxid

EG: ethylene glycol

FACS: Fluorescence Activated Cell Sorting

FU: fluorescence units

IL: Interleukin

LAF: Laminar Air flow

MNP: Micro- and nanoplastics

MP: Microplastic

mtROS: mitochondrial ROS

MTT: 3−[4,5−dimethylthiazol−2−yl] −2,5−diphenyltetrazolinum bromide

NADPH: Nicotinamide adenine dinucleotide phosphate

NF- κB: Nuclear factor kappa-light-chain-enhancer of activated B cells

NP: Nanoplastic

PBS: phosphate buffer saline

PET: polyethylene terephthalate

PET-FLUO: fluorescein-linked particles

PS: Polystyrene

ROS: reactive oxygen species

RPMI-1640: Roswell Park Memorial Institute 1640

SD: standard deviation

SDS: sodium dodecyl sulfate

TNF-α: Tumor necrose factor alpha

TPA: terephthalate acid

TPP: triphenyl phosphonium

List of figures

References

[1] C. E. Sofield, R. S. Anderton, and A. M. Gorecki, “Mind over Microplastics: Exploring Microplastic-Induced Gut Disruption and Gut-Brain-Axis Consequences,” *Curr. Issues Mol. Biol.*, vol. 46, no. 5, pp. 4186–4202, Apr. 2024, doi: 10.3390/cimb46050256.

[2] C. Yong, S. Valiyaveettil, and B. Tang, “Toxicity of Microplastics and Nanoplastics in Mammalian Systems,” *Int. J. Environ. Res. Public. Health*, vol. 17, no. 5, p. 1509, Feb. 2020, doi: 10.3390/ijerph17051509.

[3] Y. Zhou *et al.*, “Current research trends on cosmetic microplastic pollution and its impacts on the ecosystem: A review,” *Environ. Pollut.*, vol. 320, p. 121106, Mar. 2023, doi: 10.1016/j.envpol.2023.121106.

[4] B. R. Kiran, H. Kopperi, and S. Venkata Mohan, “Micro/nano-plastics occurrence, identification, risk analysis and mitigation: challenges and perspectives,” *Rev. Environ. Sci. Biotechnol.*, vol. 21, no. 1, pp. 169–203, Mar. 2022, doi: 10.1007/s11157-021-09609-6.

[5] S. Gupta *et al.*, “Atmospheric Microplastics: Perspectives on Origin, Abundances, Ecological and Health Risks,” *Environ. Sci. Pollut. Res.*, vol. 30, no. 49, pp. 107435–107464, Jul. 2023, doi: 10.1007/s11356-023-28422-y.

[6] S. Alqahtani, S. Alqahtani, Q. Saquib, and F. Mohiddin, “Toxicological impact of microplastics and nanoplastics on humans: understanding the mechanistic aspect of the interaction,” *Front. Toxicol.*, vol. 5, p. 1193386, Jul. 2023, doi: 10.3389/ftox.2023.1193386.

[7] Y.-L. Wang, C.-M. Zheng, Y.-H. Lee, Y.-Y. Cheng, Y.-F. Lin, and H.-W. Chiu, “Micro- and Nanosized Substances Cause Different Autophagy-Related Responses,” *Int. J. Mol. Sci.*, vol. 22, no. 9, p. 4787, Apr. 2021, doi: 10.3390/ijms22094787.

[8] M. Djapovic *et al.*, “Synthesis and characterization of polyethylene terephthalate (PET) precursors and potential degradation products: Toxicity study and application in discovery of novel PETases,” *Chemosphere*, vol. 275, p. 130005, Jul. 2021, doi: 10.1016/j.chemosphere.2021.130005.

[9] N. F. S. Khairul Anuar *et al.*, “An Overview into Polyethylene Terephthalate (PET) Hydrolases and Efforts in Tailoring Enzymes for Improved Plastic Degradation,” *Int. J. Mol. Sci.*, vol. 23, no. 20, p. 12644, Oct. 2022, doi: 10.3390/ijms232012644.

[10] C. M. Carr, D. J. Clarke, and A. D. W. Dobson, “Microbial Polyethylene Terephthalate Hydrolases: Current and Future Perspectives,” *Front. Microbiol.*, vol. 11, p. 571265, Nov. 2020, doi: 10.3389/fmicb.2020.571265.

[11] N. Kumar, M. Lamba, A. K. Pachar, S. Yadav, and A. Acharya, “Microplastics – A Growing Concern as Carcinogens in Cancer Etiology: Emphasis on Biochemical and

Molecular Mechanisms," *Cell Biochem. Biophys.*, Jul. 2024, doi: 10.1007/s12013-024-01436-0.

[12] K. Płuciennik, P. Sicińska, W. Misztal, and B. Bukowska, "Important Factors Affecting Induction of Cell Death, Oxidative Stress and DNA Damage by Nano- and Microplastic Particles In Vitro," *Cells*, vol. 13, no. 9, p. 768, Apr. 2024, doi: 10.3390/cells13090768.

[13] A. Banerjee and W. L. Shelver, "Micro- and nanoplastic induced cellular toxicity in mammals: A review," *Sci. Total Environ.*, vol. 755, p. 142518, Feb. 2021, doi: 10.1016/j.scitotenv.2020.142518.

[14] S. Kihara, I. Köper, J. P. Mata, and D. J. McGillivray, "Reviewing nanoplastic toxicology: It's an interface problem," *Adv. Colloid Interface Sci.*, vol. 288, p. 102337, Feb. 2021, doi: 10.1016/j.cis.2020.102337.

[15] A. Das, "The emerging role of microplastics in systemic toxicity: Involvement of reactive oxygen species (ROS)," *Sci. Total Environ.*, vol. 895, p. 165076, Oct. 2023, doi: 10.1016/j.scitotenv.2023.165076.

[16] R. Kumar *et al.*, "Micro(nano)plastics pollution and human health: How plastics can induce carcinogenesis to humans?," *Chemosphere*, vol. 298, p. 134267, Jul. 2022, doi: 10.1016/j.chemosphere.2022.134267.

[17] Y. Hong, A. Boiti, D. Vallone, and N. S. Foulkes, "Reactive Oxygen Species Signaling and Oxidative Stress: Transcriptional Regulation and Evolution," *Antioxidants*, vol. 13, no. 3, p. 312, Mar. 2024, doi: 10.3390/antiox13030312.

[18] A. A. De Souza Machado, W. Kloas, C. Zarfl, S. Hempel, and M. C. Rillig, "Microplastics as an emerging threat to terrestrial ecosystems," *Glob. Change Biol.*, vol. 24, no. 4, pp. 1405–1416, Apr. 2018, doi: 10.1111/gcb.14020.

[19] A. Jahnke *et al.*, "Reducing Uncertainty and Confronting Ignorance about the Possible Impacts of Weathering Plastic in the Marine Environment," *Environ. Sci. Technol. Lett.*, vol. 4, no. 3, pp. 85–90, Mar. 2017, doi: 10.1021/acs.estlett.7b00008.

[20] M. Hu and D. Palić, "Micro- and nano-plastics activation of oxidative and inflammatory adverse outcome pathways," *Redox Biol.*, vol. 37, p. 101620, Oct. 2020, doi: 10.1016/j.redox.2020.101620.

[21] Y. Yu *et al.*, "Roles of reactive oxygen species in inflammation and cancer," *MedComm*, vol. 5, no. 4, p. e519, Apr. 2024, doi: 10.1002/mco2.519.

[22] J.-H. Woo *et al.*, "Polypropylene nanoplastic exposure leads to lung inflammation through p38-mediated NF-κB pathway due to mitochondrial damage," *Part. Fibre Toxicol.*, vol. 20, no. 1, p. 2, Jan. 2023, doi: 10.1186/s12989-022-00512-8.

[23] T. S. Leyane, S. W. Jere, and N. N. Houreld, "Oxidative Stress in Ageing and Chronic Degenerative Pathologies: Molecular Mechanisms Involved in Counteracting

Oxidative Stress and Chronic Inflammation," *Int. J. Mol. Sci.*, vol. 23, no. 13, p. 7273, Jun. 2022, doi: 10.3390/ijms23137273.

[24] L. Rubio, R. Marcos, and A. Hernández, "Potential adverse health effects of ingested micro- and nanoplastics on humans. Lessons learned from *in vivo* and *in vitro* mammalian models," *J. Toxicol. Environ. Health Part B*, vol. 23, no. 2, pp. 51–68, Feb. 2020, doi: 10.1080/10937404.2019.1700598.

[25] J. C. Prata, "Airborne microplastics: Consequences to human health?," *Environ. Pollut.*, vol. 234, pp. 115–126, Mar. 2018, doi: 10.1016/j.envpol.2017.11.043.

[26] N. Ali, J. Katsouli, E. L. Marczylo, T. W. Gant, S. Wright, and J. Bernardino De La Serna, "The potential impacts of micro-and-nano plastics on various organ systems in humans," *eBioMedicine*, vol. 99, p. 104901, Jan. 2024, doi: 10.1016/j.ebiom.2023.104901.

[27] J. G. Calvert, "Glossary of atmospheric chemistry terms (Recommendations 1990)," *Pure Appl. Chem.*, vol. 62, no. 11, pp. 2167–2219, Jan. 1990, doi: 10.1351/pac199062112167.

[28] L. Rodriguez De La Fuente, A. M. K. Law, D. Gallego-Ortega, and F. Valdes-Mora, "Tumor dissociation of highly viable cell suspensions for single-cell omic analyses in mouse models of breast cancer," *STAR Protoc.*, vol. 2, no. 4, p. 100841, Dec. 2021, doi: 10.1016/j.xpro.2021.100841.

[29] R. Pascua-Maestro, M. Corraliza-Gomez, S. Diez-Hermano, C. Perez-Segurado, M. D. Ganfornina, and D. Sanchez, "The MTT-formazan assay: Complementary technical approaches and in vivo validation in Drosophila larvae," *Acta Histochem.*, vol. 120, no. 3, pp. 179–186, Apr. 2018, doi: 10.1016/j.acthis.2018.01.006.

[30] M. Ghasemi, T. Turnbull, S. Sebastian, and I. Kempson, "The MTT Assay: Utility, Limitations, Pitfalls, and Interpretation in Bulk and Single-Cell Analysis," *Int. J. Mol. Sci.*, vol. 22, no. 23, p. 12827, Nov. 2021, doi: 10.3390/ijms222312827.

[31] D. Figueroa, M. Asaduzzaman, and F. Young, "Real time monitoring and quantification of reactive oxygen species in breast cancer cell line MCF-7 by 2′,7′–dichlorofluorescin diacetate (DCFDA) assay," *J. Pharmacol. Toxicol. Methods*, vol. 94, pp. 26–33, Nov. 2018, doi: 10.1016/j.vascn.2018.03.007.

[32] A. Keller, A. Mohamed, S. Dröse, U. Brandt, I. Fleming, and R. P. Brandes, "Analysis of Dichlorodihydrofluorescein and Dihydrocalcein as Probes for the Detection of Intracellular Reactive Oxygen Species," *Free Radic. Res.*, vol. 38, no. 12, pp. 1257–1267, Dec. 2004, doi: 10.1080/10715760400022145.

[33] S. Kalinovic *et al.*, "Comparison of Mitochondrial Superoxide Detection Ex Vivo/In Vivo by mitoSOX HPLC Method with Classical Assays in Three Different Animal Models of

Oxidative Stress," *Antioxidants*, vol. 8, no. 11, p. 514, Oct. 2019, doi: 10.3390/antiox8110514.

[34] J. Zielonka *et al.*, "Cytochrome c-mediated oxidation of hydroethidine and mito-hydroethidine in mitochondria: Identification of homo- and heterodimers," *Free Radic. Biol. Med.*, vol. 44, no. 5, pp. 835–846, Mar. 2008, doi: 10.1016/j.freeradbiomed.2007.11.013.

[35] A. Kafkova and J. Trnka, "Mitochondria-targeted compounds in the treatment of cancer," *Neoplasma*, vol. 67, no. 03, pp. 450–460, 2020, doi: 10.4149/neo_2020_190725N671.

[36] K. Duval *et al.*, "Modeling Physiological Events in 2D vs. 3D Cell Culture," *Physiology*, vol. 32, no. 4, pp. 266–277, Jul. 2017, doi: 10.1152/physiol.00036.2016.

[37] O. Habanjar, M. Diab-Assaf, F. Caldefie-Chezet, and L. Delort, "3D Cell Culture Systems: Tumor Application, Advantages, and Disadvantages," *Int. J. Mol. Sci.*, vol. 22, no. 22, p. 12200, Nov. 2021, doi: 10.3390/ijms222212200.

[38] E. Brynzak-Schreiber *et al.*, "Microplastics role in cell migration and distribution during cancer cell division," *Chemosphere*, vol. 353, p. 141463, Apr. 2024, doi: 10.1016/j.chemosphere.2024.141463.

[39] L. Ma *et al.*, "Differences in toxicity induced by the various polymer types of nanoplastics on HepG2 cells," *Sci. Total Environ.*, vol. 918, p. 170664, Mar. 2024, doi: 10.1016/j.scitotenv.2024.170664.

[40] M. L. Circu and T. Y. Aw, "Reactive oxygen species, cellular redox systems, and apoptosis," *Free Radic. Biol. Med.*, vol. 48, no. 6, pp. 749–762, Mar. 2010, doi: 10.1016/j.freeradbiomed.2009.12.022.

[41] T. Zaidieh, J. R. Smith, K. E. Ball, and Q. An, "ROS as a novel indicator to predict anticancer drug efficacy," *BMC Cancer*, vol. 19, no. 1, p. 1224, Dec. 2019, doi: 10.1186/s12885-019-6438-y.

[42] S. A. Meredith, Y. Kusunoki, S. D. Connell, K. Morigaki, S. D. Evans, and P. G. Adams, "Self-Quenching Behavior of a Fluorescent Probe Incorporated within Lipid Membranes Explored Using Electrophoresis and Fluorescence Lifetime Imaging Microscopy," *J. Phys. Chem. B*, vol. 127, no. 8, pp. 1715–1727, Mar. 2023, doi: 10.1021/acs.jpcb.2c07652.

[43] S. A. Langhans, "Three-Dimensional in Vitro Cell Culture Models in Drug Discovery and Drug Repositioning," *Front. Pharmacol.*, vol. 9, p. 6, Jan. 2018, doi: 10.3389/fphar.2018.00006.

[44] G. Halimu *et al.*, "Toxic effects of nanoplastics with different sizes and surface charges on epithelial-to-mesenchymal transition in A549 cells and the potential toxicological

mechanism," *J. Hazard. Mater.*, vol. 430, p. 128485, May 2022, doi: 10.1016/j.jhazmat.2022.128485.

[45] H. Wu, T. Xu, T. Chen, J. Liu, and S. Xu, "Oxidative stress mediated by the TLR4/NOX2 signalling axis is involved in polystyrene microplastic-induced uterine fibrosis in mice," *Sci. Total Environ.*, vol. 838, p. 155825, Sep. 2022, doi: 10.1016/j.scitotenv.2022.155825.

[46] W. Wang, A. T. N. Do, and J.-H. Kwon, "Ecotoxicological effects of micro- and nanoplastics on terrestrial food web from plants to human beings," *Sci. Total Environ.*, vol. 834, p. 155333, Aug. 2022, doi: 10.1016/j.scitotenv.2022.155333.

[47] A. P. Walczak *et al.*, "Bioavailability and biodistribution of differently charged polystyrene nanoparticles upon oral exposure in rats," *J. Nanoparticle Res.*, vol. 17, no. 5, p. 231, May 2015, doi: 10.1007/s11051-015-3029-y.

[48] Y. He *et al.*, "Cytotoxic effects of polystyrene nanoplastics with different surface functionalization on human HepG2 cells," *Sci. Total Environ.*, vol. 723, p. 138180, Jun. 2020, doi: 10.1016/j.scitotenv.2020.138180.

[49] A. Weber *et al.*, "Nanoplastics affect the inflammatory cytokine release by primary human monocytes and dendritic cells," *Environ. Int.*, vol. 163, p. 107173, May 2022, doi: 10.1016/j.envint.2022.107173.